Highlights of the production of (anti-)(hyper-)nuclei and exotica with ALICE at the LHC

Benjamin Dönigus (for the ALICE Collaboration)

Institut für Kernphysik, Goethe-Universität Frankfurt, Max-von-Laue-Str. 1, 60438 Frankfurt, Germany

E-mail: benjamin.doenigus@cern.ch

Abstract. Measurements of the production of light (anti-)nuclei and (anti-)hypernuclei have been performed in different colliding systems at the LHC, namely pp, p–Pb and Pb–Pb. The results of the production in Pb–Pb collisions of light (anti-)(hyper-)nuclei follows the expectation of the thermal model, whereas the production of nuclei in pp and p–Pb collisions shows a closer agreement with the expectations from coalescence models. Both models can give predictions for the production yields of hypothetical states such as bound states of two Λ hyperons or of a Λ and a neutron, which are expected to decay weakly. These states are searched for with the ALICE apparatus. Since no signal is found, upper limits, which are significantly below the model expectations, are set. Furthermore, the most recent measurement of the lifetime of the hypertriton determined in Pb–Pb collisions at $\sqrt{s_{\rm NN}} = 5.02$ TeV at the LHC gives a value exactly between the world average and the free Λ lifetime. In addition, the new result is in agreement with other recent measurements in heavy-ion collisions.

1. Introduction

The ALICE (A Large Ion Collider Experiment) Collaboration has, in addition to the usual heavy-ion physics research, developed a program to investigate many different kinds of (multi-)baryon states predicted by QCD and QCD inspired models [1]. One way of addressing this research topic is to start by measuring rarely observed (anti-)nuclei and (anti-)hypernuclei, which are measured copiously in Pb–Pb collisions at the LHC due to the large data sets. With these data the model predictions, e.g. the thermal (statistical) model and coalescence approaches, can be tested. Ultimately, the aim is to understand the production mechanisms at play in these collisions, resulting in large production yields for (anti-)nuclei and (anti-)hypernuclei. Furthermore, one can then use these models to predict the production yields of exotic bound states, still to be discovered or excluded, by setting strong upper limits, compared to these models.

The main assumption of the thermal (statistical) model used in the following is a grand-canonical ensemble, which is characterized by three parameters, temperature, (baryon) chemical potential and volume. In this approach all production yields of light flavored hadrons (containing only u, d and s quarks) are described by these three parameters through the grand-canonical partition function [2,3]. The thermal model at the LHC has basically only one key parameter: the chemical freeze-out temperature T_{ch}. This statement is valid because the baryo-chemical potential μ_B is close to zero, and therefore it is often treated as being zero in thermal model fits. The nuclei themselves are subject to a strong sensitivity on T_{ch}, because of their large mass and the exponential behaviour of the expected particle yields $\mathrm{d}N/\mathrm{d}y$ on the particle mass m

($\mathrm{d}N/\mathrm{d}y \propto \exp(-m/T_{ch})$). The interesting fact to mention here is that the binding energies of these objects are very small compared to the chemical freeze-out temperature T_{ch} [2,3,4].

In the coalescence approach, the constituents of a (hyper-)nucleus, produced from the fireball, are expected to come close together in phase space and finally form the (hyper-)nucleus. In this model the produced nuclei could break apart and be created again by final-state coalescence.

More details and the current status of these two different production models, connected to the here presented data, are given in [5].

The measured cross-section in heavy-ion collisions is often split into so called centrality intervals or classes. These are extracted from Monte-Carlo simulations to model the fraction of the cross-section as a percentage of the total cross-section based on detectors in the forward direction. In nucleus-nucleus collisions, these intervals are interpreted as a proxy for the degree of centrality of the collision. This interpretation is no longer true for pp or p–Pb collisions, where the cross-section is divided in multiplicity classes.

2. (Anti-)nuclei

The measurement of (anti-)nuclei is performed by the ALICE experiment by using the Time Projection Chamber (TPC) and the Time-Of-Flight detector (TOF). The TOF is used in addition whenever the TPC is not sufficient to separate the different nuclei from other hadrons using the specific energy-loss $\mathrm{d}E/\mathrm{d}x$. One way to combining the information of both detectors is to measure the mass of the investigated particle. This is accomplished by using the velocity $\beta = \mathrm{v}/c$ given by TOF and the measured momentum (mainly determined by the curvature of the track in the TPC), for a pre-selection of particles which are based on the TPC $\mathrm{d}E/\mathrm{d}x$ measurement. A result of the measured $(m/z)^2$ for $^3\overline{\mathrm{He}}$ and $^4\overline{\mathrm{He}}$ in Pb–Pb collisions at $\sqrt{s_{\mathrm{NN}}} = 5.02$ TeV is shown in Fig. 1. This figure shows that the data sample of 2015 contains 16 clearly identifed anti-alphas, by using the TPC and TOF information.

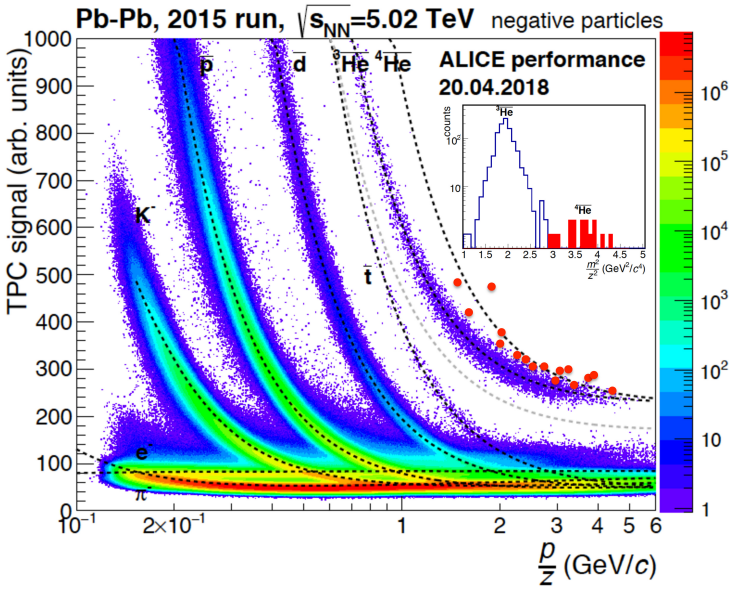

Figure 1. $\mathrm{d}E/\mathrm{d}x$ for negative tracks, measured in the ALICE TPC, of events containing at least one particle with $|Z| > 1$ (selected by requiring only events where one particle is found above the grey dashed line between $\bar{\mathrm{t}}$ and $^3\overline{\mathrm{He}}$). All light nuclei are clearly visible and shown together with the parameterization of the Bethe-Bloch expectation. The inset also shows the mass obtained by combining the measured time-of-flight and rigidity p/z, for a 3σ selection of alphas in the TPC.

Furthermore, spectra are extracted by dividing the signal in p_{T} slices and correcting them for acceptance and efficiency. The result for deuterons in pp collisions at $\sqrt{s} = 7$ TeV and for five different centrality bins in Pb–Pb at $\sqrt{s_{\mathrm{NN}}} = 2.76$ TeV is displayed in Fig. 2, together with the ratios of the anti-nuclei to nuclei in the same centrality classes. In addition, this ratio is also shown for ^{3}He. All ratios are compatible with unity as a function of transverse momentum as expected from thermal and coalescence models. Thus, nuclei and anti-nuclei are produced with equal probability at the LHC [4].

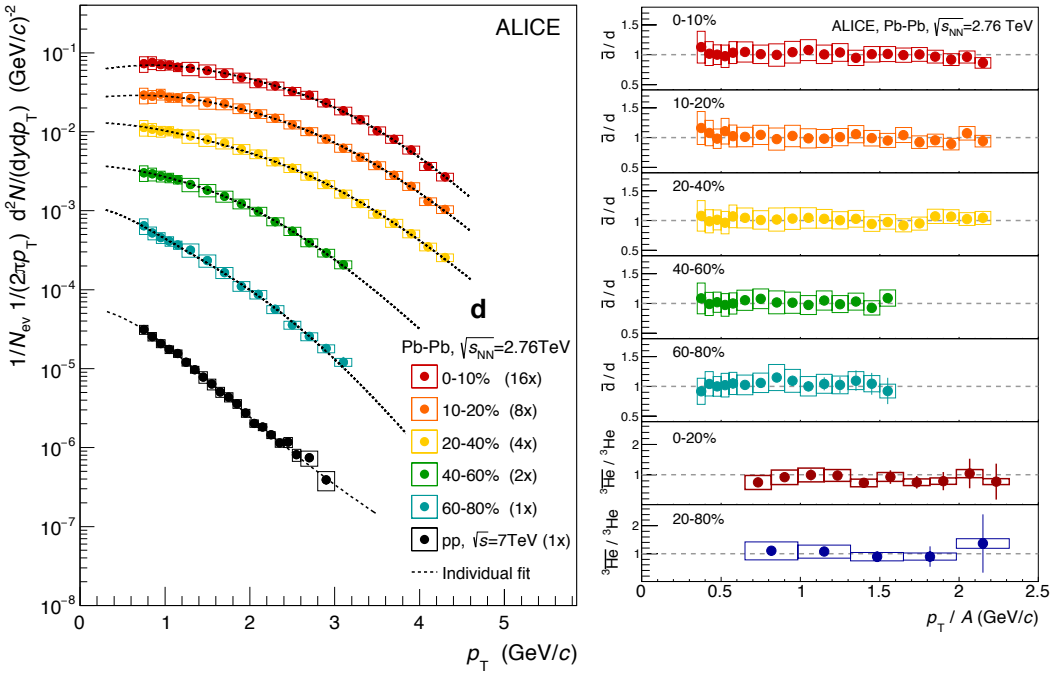

Figure 2. Invariant transverse momentum spectra for deuterons in pp at $\sqrt{s} = 7$ TeV and 10 centrality classes in Pb–Pb at $\sqrt{s_{\mathrm{NN}}} = 2.76$ TeV (left panel) and ratio between anti-nuclei and nuclei ($\bar{\mathrm{d}}$/d and $^3\overline{\mathrm{He}}/^3$He) for the different centrality classes in the right panel. Figures are taken from [8].

The spectra in Pb–Pb show a clear hardening (higher mean p_{T}) with increasing centrality and they are fitted with blast-wave distributions [6], mainly to extrapolate to the unmeasured region of the spectra in order to extract the integrated production yield. The blast-wave function is used to take into account the radial push, the so called radial flow, all particles are exposed to in a heavy-ion collision during the evolution of the fireball.

The development of the radial flow from minimum bias pp events towards the Pb–Pb centrality intervals is even better visible in the data at higher energies, namely the pp collisions at $\sqrt{s} = 13$ TeV and Pb–Pb at $\sqrt{s_{\mathrm{NN}}} = 5.02$ TeV, representing the current top energies in these colliding systems at the LHC. The aforementioned effect is displayed in Fig. 3 (left), together with the pp data split in multiplicity intervals, where a similar hardening can be seen.

The ratios of the production yields of deuterons to protons in pp, p–Pb and Pb–Pb collisions as a function of the mean multiplicity $\langle \mathrm{d}N_{\mathrm{ch}}/\mathrm{d}\eta \rangle$ are depicted in Fig. 4. These show an increase going from pp multiplicities over p-Pb multiplicities until a saturation seems to be reached in peripheral Pb–Pb collisions. The increase with multiplicity is predicted by coalescence models whereas the basically constant behaviour at higher multiplicities is expected from the thermal

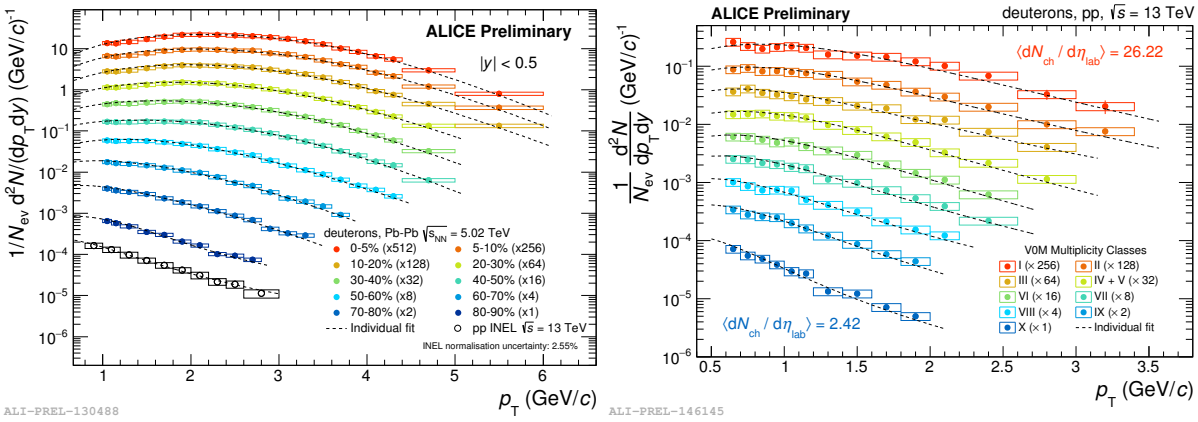

Figure 3. Transverse momentum spectra for deuterons in pp at $\sqrt{s} = 13$ TeV and five centrality classes in Pb–Pb at $\sqrt{s_{\rm NN}} = 5.02$ TeV (left panel) and transverse momentum spectra for deuterons in pp at $\sqrt{s} = 13$ TeV split in 9 different multiplicity classes (right panel). The dashed lines indicate individual fits to the data, for pp using a Levy-Tsallis function [9,10,11] and in Pb–Pb using a blast-wave function.

model.

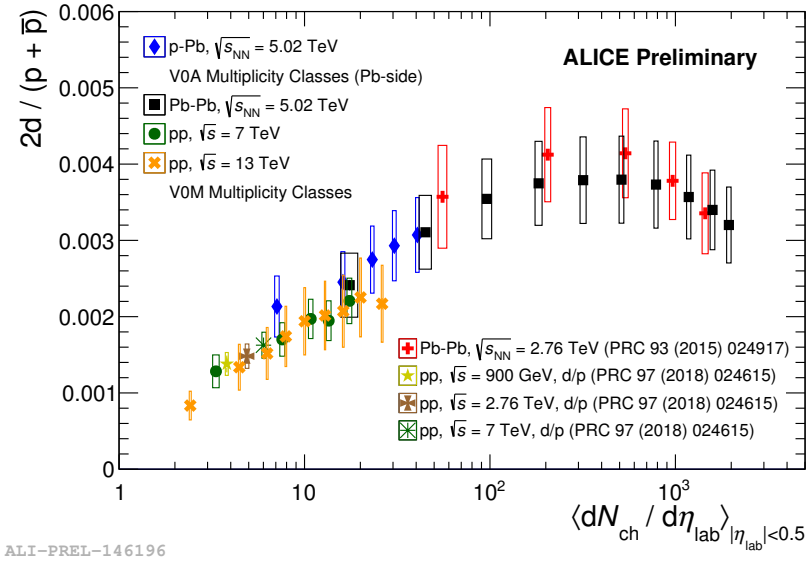

Figure 4. Ratios of the production yields of deuterons to protons ($2d/(p+\bar{p})$) as a function of the mean multiplicity $\langle dN_{\rm ch}/d\eta \rangle$ measured in pp, p–Pb and Pb–Pb collisions at different energies.

Figure 5 shows the production yield of nuclei in Pb–Pb and p–Pb collisions as a function of their mass together with exponential fits. As mentioned above an exponential decrease with mass is expected from the thermal model. The penalty factor for adding a baryon to the system is about 300 in Pb–Pb and around 600 in p-Pb, which would mean that the suppression in the yields of d to ^{3}He is 300 in Pb–Pb and 600 in p–Pb.

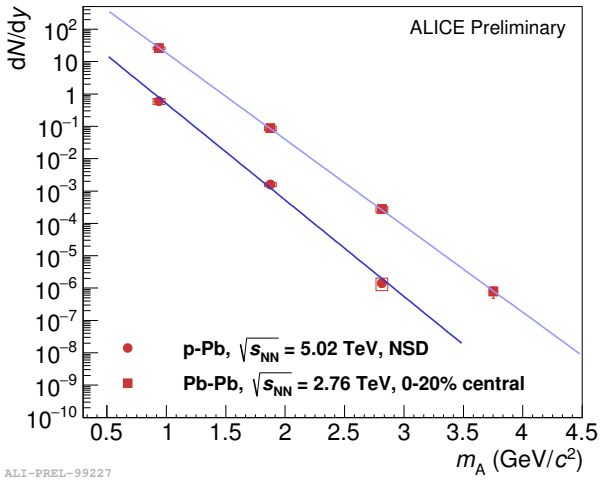

Figure 5. Production yields of different nuclei as a function of their mass. The lines indicate exponential fits through the data points at the two energies.

Figure 6 displays the production yields of different light flavour particle species compared to three different thermal model fits from three different model implementations. These model fits agree very well with each other. From these fits a temperature T_{ch} of about 153 MeV can be extracted. All nuclei and hypernuclei production yields are rather well described with this model. The biggest tension in this fit is visible for the K*, which is a strongly-decaying resonance with a lifetime shorter than the lifetime of the fireball. This result will be discussed in more detail in Sec. 5.

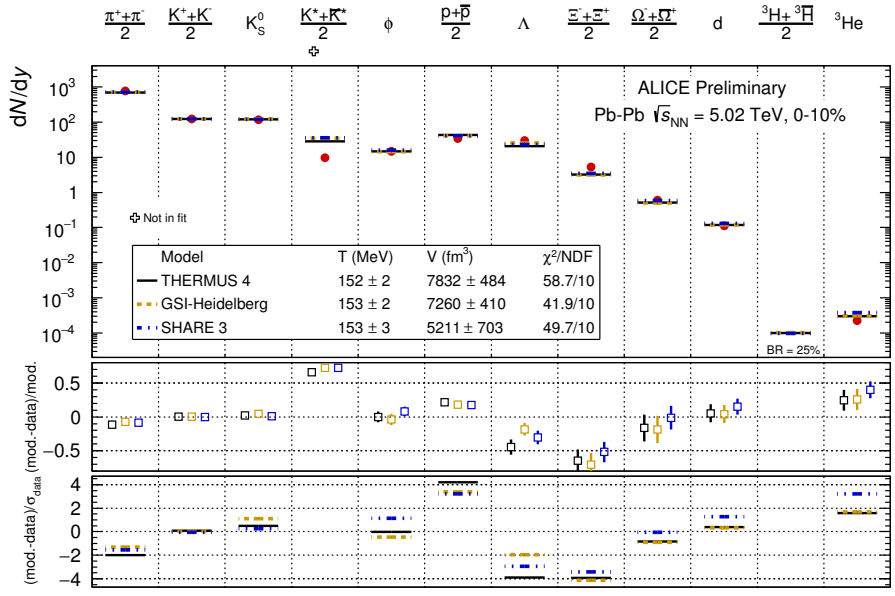

Figure 6. Production yields of different light flavour particle species compared to three different thermal model implementations.

3. (Anti-)hypernuclei

The hypertriton is the lightest hypernucleus, consisting of a proton, a neutron and a Λ hyperon. It decays weakly, for instance by its two-body decay mode into a ^{3}He and a π^-, with a lifetime close to the one of the free Λ hyperon. The separation energy of the Λ is only 130 keV, which implies, from simple quantum mechanical calculations, that the hypertriton has a size of about 10 fm [5]. This already indicates that the lifetime should be very close to the one of the free Λ. A similar prediction is given by a more sophisticated model involving also three-body forces [7]. In addition, this model gives a branching ratio of the hypertriton decay into the ^{3}He+π^- of about 25%. The branching ratios (B.R.) of the hypertriton decay modes are not well known because many channels involve neutral particles such as neutrons and π^0 that are not easily accessible by production experiments. The most recent calculation includes also the modelling of the π final-state interaction, which leads to a value very close to the current world average (about 81% of the free Λ hyperon lifetime) [12]. First results on the hypertriton by the ALICE Collaboration were published in [13].

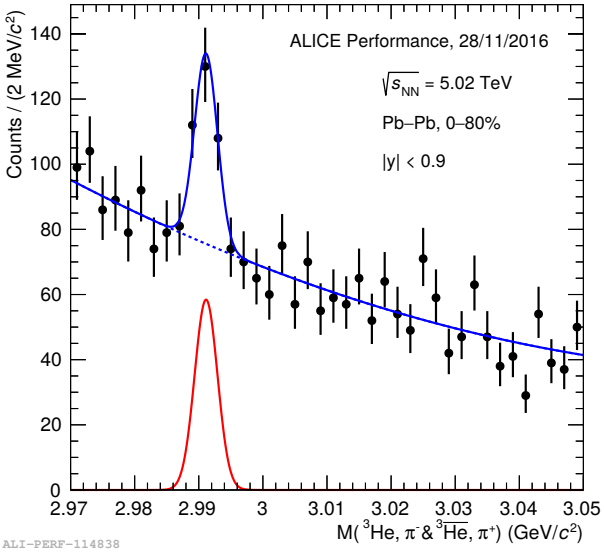

Figure 7. Invariant mass of the hypertriton, reconstructed by using a secondary decay topology of a ^{3}He and π^- together with their charge conjugate from the 2015 data sample.

The reconstructed invariant mass of the hypertriton in 0-80% central Pb–Pb collisions at $\sqrt{s_{\rm NN}}$ = 5.02 TeV is shown in Fig. 7. The extracted signal is fitted by a Gaussian and the extracted mass is $m = (2.991 \pm 0.001)$ GeV/c^2 and the width $\sigma = (1.7 \pm 0.3)$ MeV/c^2. From such fits to invariant mass distributions, differential analyses in centrality and $p_{\rm T}$ are performed.

The measured transverse momentum spectrum of the hypertriton (red points) and anti-hypertriton (blue points) in 10-40% central Pb–Pb events at $\sqrt{s_{\rm NN}}$ = 5.02 TeV are shown in Fig. 8, together with blast-wave functions based on the measurement of light nuclei. The fact that these spectra can be parameterised by blast-wave functions indicates that the hypertriton experiences the same flow and the same evolution as all other particles produced in the hot fireball.

The measured dN/dy×B.R. of the hypertriton in 0-10% central Pb–Pb collisions at $\sqrt{s_{\rm NN}}$ = 5.02 TeV as a function of the branching ratio is depicted in Fig. 9, together with model calculations describing its production. The thermal model, which describes well the production of light hadrons and nuclei, is in agreement with the measurement around the 25% branching ratio expected from the previously mentioned calculation.

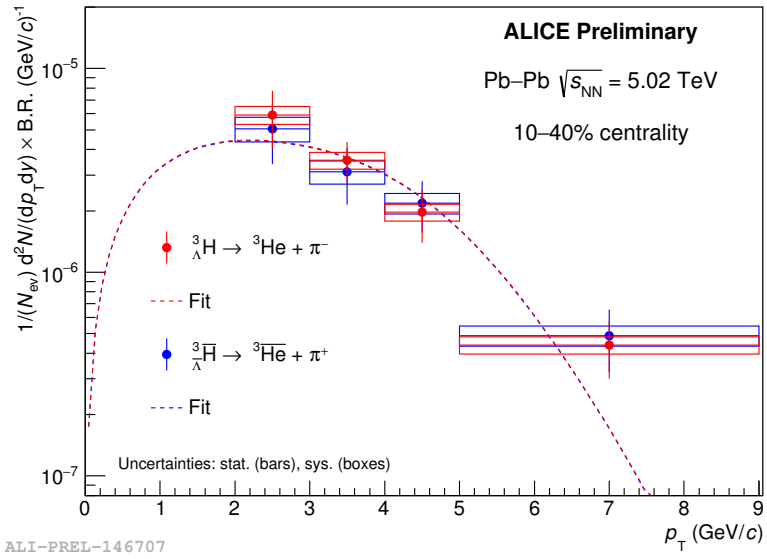

Figure 8. Transverse momentum spectrum of the hypertriton in 10-40% central Pb–Pb events at $\sqrt{s_{\rm NN}} = 5.02$ TeV. The dashed lines are blast-wave functions based on the measurement of light nuclei.

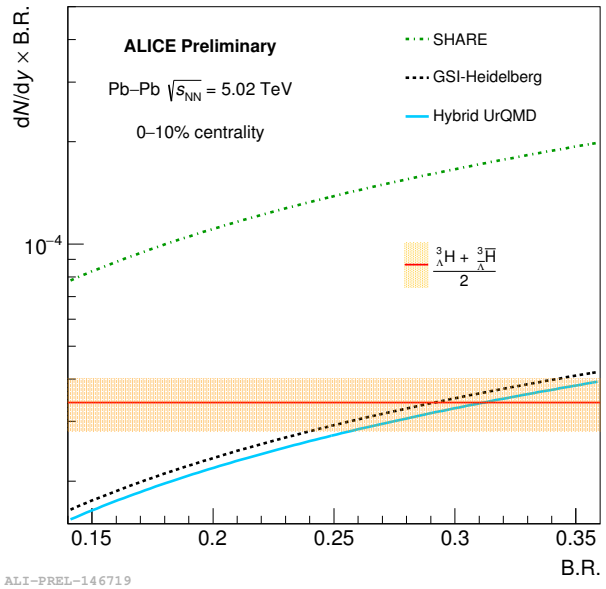

Figure 9. $p_{\rm T}$-integrated rapidity density times branching ratio as a function of branching ratio (dN/dy×B.R. vs B.R.). The red horizontal line is the measured dN/dy×B.R. and the band around it represents the quadratic sum of statistical and systematic uncertainties. The other lines indicate different theoretical expectations.

The extracted lifetime is displayed in Fig. 10 and compared with previous measurements. An average lifetime calculated following the PDG description, which deviates from the free Λ

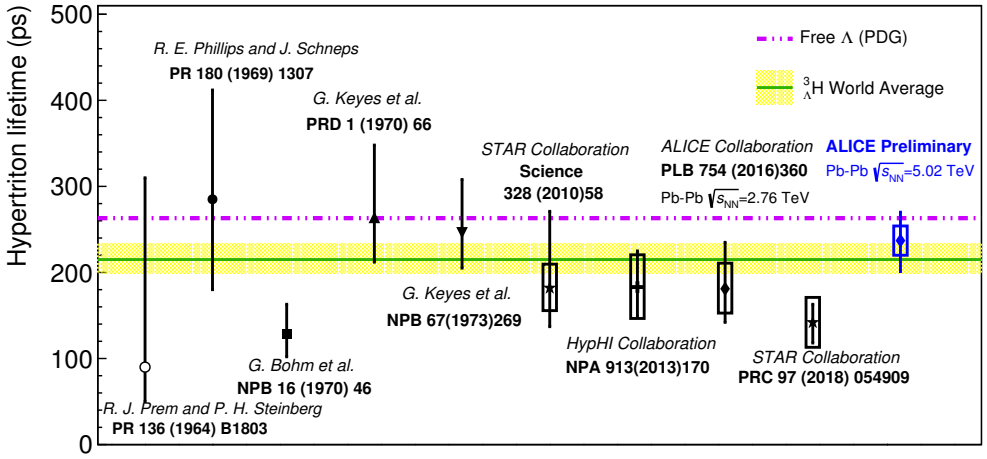

ALI-DER-161043

Figure 10. Measured hypertriton lifetime (blue symbol) compared to previously published results (in black). The yellow band represents the world average of the hypertriton lifetime measurements. The dashed line indicates the lifetime of the Λ hyperon as reported by the Particle Data Group.

hyperon lifetime by more than 2σ, is also shown. The measurements before 2010 were done with visualization techniques (emulsions and bubble chambers) whereas the latest ones are all from heavy-ion collisions. The fact that the lifetimes extracted from heavy-ion collisions are lower than the lifetime of the free Λ hyperon leads to the suggestion, in the hyper-nuclei community, that the measurements in heavy-ion collisions might be biased because of the the rougher collision environment, which could influence the observed lifetime of the hypertriton. In particular, the most recent value from the STAR Collaboration [14] is more than 3σ below the free Λ lifetime. Therefore measurements of the lifetime in elementary collisions are desirable.

An unbinned fit was used as cross-check of the result from the exponential fit in ct bins. This unbinned fit is shown in Fig. 11. With this method sideband regions are used for fitting the background and the signal region for extracting the lifetime of the hypertriton.

4. Exotica searches

Since the production yields of composite objects (such as light (anti-)(hyper-)nuclei) are rather well described by both production models they can be used to predict the production of exotic objects such as bound states among hyperons or hyperons and nucleons. Of particular interest is the so-called H-dibaryon, a hexaquark state composed of $uuddss$ (ΛΛ) predicted by R. Jaffe in a bag model calculation in 1977 [15]. It is investigated in the weak decay mode $\Lambda + \mathrm{p} + \pi^-$. Another investigated bound state is a possible bound state of Λn that would decay into $\mathrm{d} + \pi^-$. Since no signal was observed, upper limits have been extracted for a wide phase space of lifetime and branching ratio.

The upper limits of the investigated bound states are depicted in Fig. 12 as a function of the branching ratio assuming the same lifetime of the free Λ hyperon. All production models are far away from the extracted upper limits in reasonable regions of the branching ratio. Only if the branching ratios were very small, the model predictions would reach down to the upper-limit value.

The dependency of the upper limit on the lifetime is displayed in Fig. 13 and shows that only

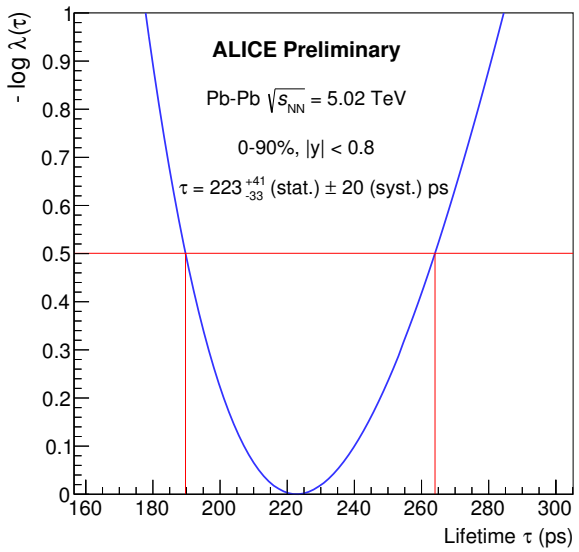

Figure 11. Negative logarithmic likelihood of the measured hypertriton lifetime from the unbinned fit method.

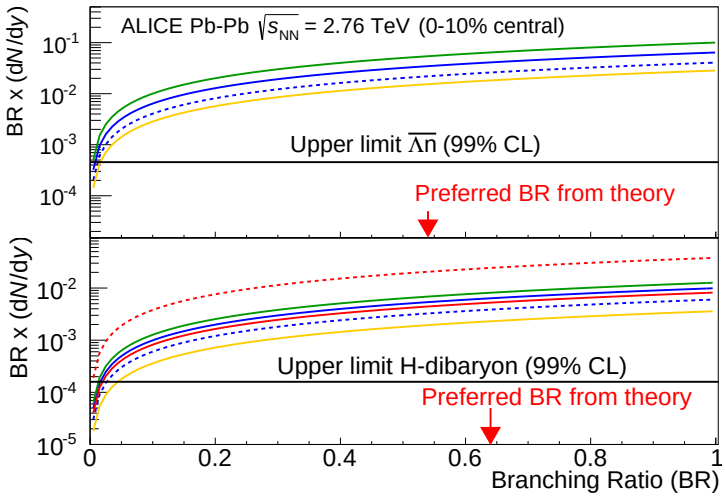

Figure 12. Extracted upper limit $\mathrm{d}N/\mathrm{d}y$ as a function of the branching ratio compared with different models. For details see [16].

at very long lifetimes (about 3 m) the upper limit of the H-dibaryon comes close to the thermal model expectation. For the Λn bound state the upper limits are for all configurations under study below the model expectation. More details are given in [16].

5. Resonances

In Fig. 6 one can see a deviation for the K*(892) when the measured production yield is compared to the thermal model expectation. On the other hand, the measured $\phi(1020)$ production yield is well compatible with the thermal model. This can be understood from the different lifetimes

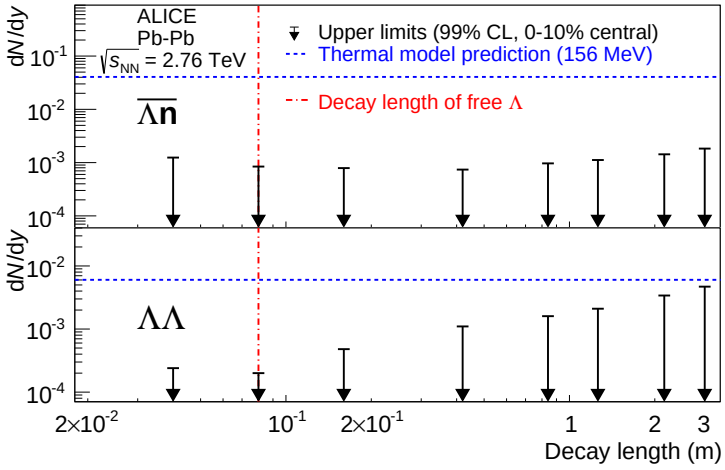

Figure 13. Upper limit $\mathrm{d}N/\mathrm{d}y$ as a function of the decay length compared with the the thermal model. For details see [16].

of the two resonances, namely 46.1 fm/c for the $\phi(1020)$ and 4.2 fm/c for the K*(892). These are respectively longer and shorter than the lifetime of the fireball which is about 10 fm/c for central heavy-ion collisions at the LHC. Consequently some of the K*(892) are decaying already inside the expanding fireball and interact with it, so that these K*(892) can not be reconstructed anymore. This can be seen in Fig. 14 from the ratio of K*(892) to K$^-$, which decreases as the number of produced charged particles (here as $\langle \mathrm{d}N_{\mathrm{ch}}/\mathrm{d}\eta \rangle^{1/3}$) increases (going from pp multiplicity towards central Pb–Pb events). At the same time the ratio of $\phi(1020)$ to K$^-$ stays rather constant. One can see that at low multiplicities the measured values agree with the thermal model.

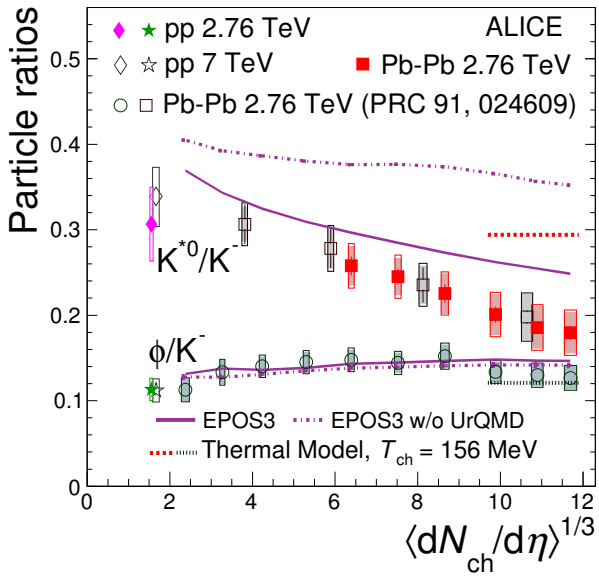

Figure 14. Ratio of K*(892) to K$^-$ and $\phi(1020)$ to K$^-$ as function of $\langle \mathrm{d}N_{\mathrm{ch}}/\mathrm{d}\eta \rangle^{1/3}$ compared to different models. For details see [17].

6. Summary and outlook

The results from the production of (anti-)nuclei (in pp, p–Pb and Pb–Pb collisions) and (anti-)hypernuclei (in Pb–Pb collisions) are described rather well by the thermal and the coalescence models, whereas some aspects in pp and p–Pb are in closer agreement to coalescence than thermal models. Both models can make predictions for the production of exotic objects, such as the H-dibaryon and a Λn bound state. Since in the search of these exotica no signals were observed, upper limits were set which are significantly below the expectations of both models. A comparison of the thermal model involving all discussed states is displayed in Fig. 15. It shows that the thermal model describes the yields of the known states very well. Even the hypertriton, which has a Λ separation energy of only 130 keV, is in good agreement. Instead, the upper limits of the exotic states are more than a factor of 25 below the expectation. This makes the existence of these particles in the investigated phase space rather unlikely.

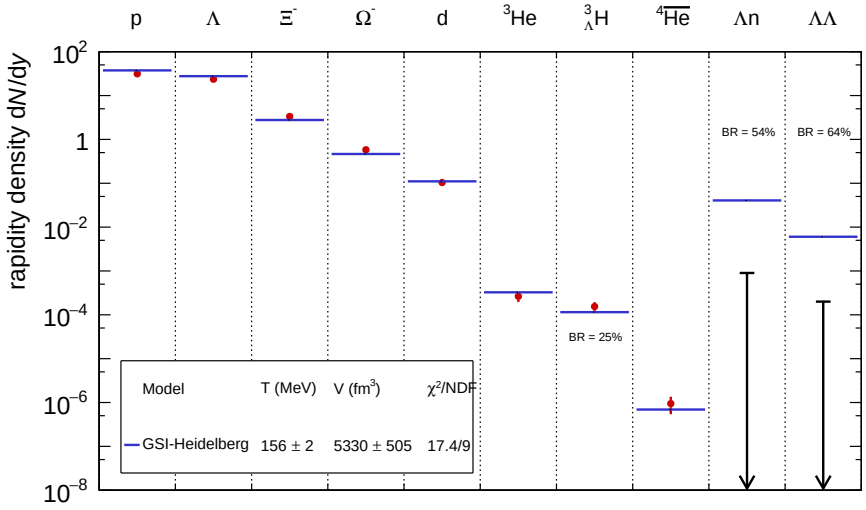

Figure 15. Comparison of production yields $\mathrm{d}N/\mathrm{d}y$ of baryons, light (hyper-)nuclei and exotica with thermal model predictions. Hypertriton was corrected by 25% for the branching ratio, Λn by 54% and ΛΛ by 64% as shown in [18].

Further, the most recent measurement of the lifetime of the hypertriton, determined in Pb–Pb collisions at $\sqrt{s_{\mathrm{NN}}} = 5.02$ TeV at the LHC, gives a value around the expectations of the most recent calculation [12] and it is consistent with the free Λ hyperon lifetime and the world average. Thus it is in agreement with other recent measurements in heavy-ion collisions and from emulsions. The repeat of this measurement in more elementary collisions is one of the aims of run 2, which started in 2015 and will deliver significantly larger data sets at higher collision energies as before ($\sqrt{s} = 13$ TeV in pp).

After 2018 in the so-called long shutdown 2 (LS2) two main detectors of the ALICE setup will be upgraded. The current Inner Tracker, consisting of six layers of silicon detectors based on three different technologies, will be replaced by a new tracker made of seven layers of monolithic silicon pixel sensors that will significantly increase the (secondary) vertex resolution [19]. The multi-wire proportional chambers of the TPC will be replaced by four layers of GEM detectors that will allow for continuous readout at rates of 50 kHz [20]. These upgrades will allow the ALICE detector to cope with the higher luminosity expected in run 3 (starting in 2021) and run 4 (starting in 2026). In runs 3 and 4, a data sample of 10^{10} central Pb–Pb events corresponding to 10 nb^{-1} integrated luminosity is expected to be collected. This sample will allow to study the production of the particles presented here with higher precision and will allow ALICE to

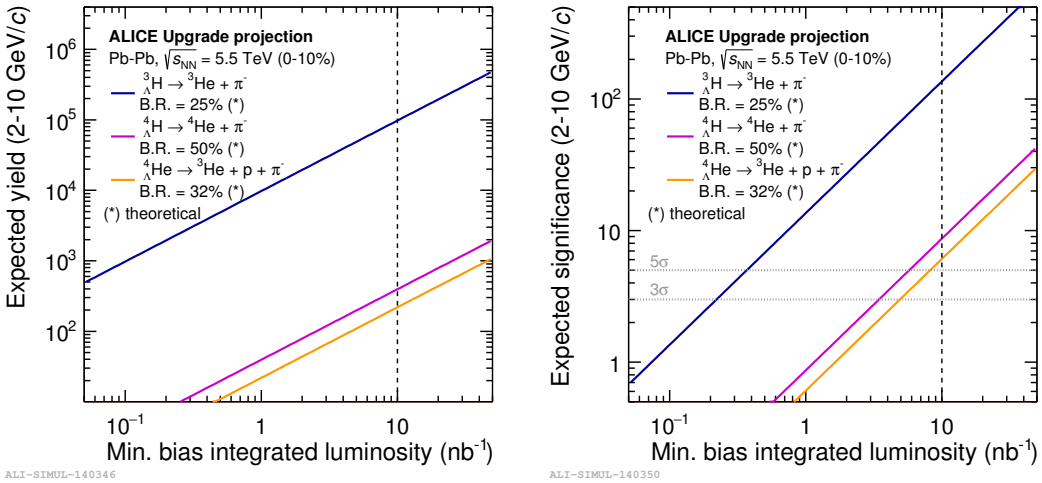

Figure 16. Expected yields of hyper-nuclei ($^{3}_{\Lambda}$H, $^{4}_{\Lambda}$H and $^{4}_{\Lambda}$He) in 0-10% central Pb–Pb collisions in runs 3 and 4 as a function of the integrated minimum bias luminosity (left panel). Expected significance of hyper-nuclei ($^{3}_{\Lambda}$H, $^{4}_{\Lambda}$H and $^{4}_{\Lambda}$He) in 0-10% central Pb-Pb collisions in runs 3 and 4 as a function of the integrated minimum bias luminosity (right panel). The vertical dashed line represents the target luminosity of 10 nb^{-1}. The horizontal dashed lines at 3σ and 5σ help to guide the eye.

study also hyper-nuclei with A=4 as indicated in Fig. 16.

7. Acknowledgments

The author acknowledges the support from the German Bundesministerium für Bildung, Wissenschaft, Forschung und Technologie (BMBF) though the project grant 05P2015 - ALICE at High Rate (BMBF-FSP202) (Förderkennzeichen 05P15RFCA1).

8. References

[1] Abelev B et al. (ALICE Collaboration), 2014 *J. Phys. G: Nucl. Part. Phys.* **41** 087001
[2] Andronic A et al., 2018 *Nature* **561** 321
[3] Andronic A et al., 2011 *Phys. Lett. B* **697** 203
[4] Cleymans J et al., 2011 *Phys. Rev. C* **84** 054916
[5] Braun-Munzinger P, Dönigus B, 2019 *Nucl. Phys. A* **987** 144
[6] Schnedermann E et al., 1993 *Phys. Rev. C* **48** 2462
[7] Kamada H et al., 1998 *Phys. Rev. C* **57** 1595
[8] Adam J et al. (ALICE Collaboration), 2016 *Phys. Rev. C* **93** 02491
[9] Tsallis C, 1988 *J. Statist. Phys.* **52** 479
[10] Abelev B.I. et al. (STAR Collaboration), 2007 *Phys. Rev. C* **75** 064901
[11] Cleymans J, Worku D, 2012 *J. Phys. G: Nucl. Part. Phys.* **39** 025006
[12] Gal A, Garzilaco H, 2019 *Phys. Lett. B* **791** 48
[13] Adam J et al. (ALICE Collaboration), 2016 *Phys. Lett. B* **754** 360
[14] Adamczyk L et al. (STAR Collaboration), 2018 *Phys. Rev. C* **97** 054909
[15] Jaffe R L, 1977 *Phys. Rev. Lett.* **38** 195 and 617
[16] Adam J et al. (ALICE Collaboration), 2016 *Phys. Lett. B* **752** 267
[17] Adam J et al. (ALICE Collaboration), 2017 *Phys. Rev. C* **95** 064606
[18] Braun-Munzinger P, Dönigus B, Löher N, 2015 *CERN Courier* **September**
[19] Abelev B et al. (ALICE Collaboration), 2014 *J. Phys. G* **41** 087002
[20] Adam J et al. (ALICE Collaboration), 2014 *CERN-LHCC-2013-020, ALICE-TDR-016*